Determination of p-y Curves for Bucket Foundations in Sand Using Finite Element Modeling

Knudsen, Bjørn S.; Østergaard, Martin Underlin; Ibsen, Lars Bo; Clausen, Johan

Publication date:
2013

Document Version
Publisher's PDF, also known as Version of record

Determination of p-y Curves for Bucket Foundations in Sand Using Finite Element Modeling

Bjørn Staghøj Knudsen
Martin Underlin Østergaard
Lars Bo Ibsen
Johan Clausen

ISSN 1901-7278
DCE Technical Memorandum No. 31

DEPARTMENT OF CIVIL ENGINEERING
AALBORG UNIVERSITY

Aalborg University
Department of Civil Engineering

DCE Technical Memorandum No. 31

Determination of p-y Curves for Bucket Foundations in Sand Using Finite Element Modeling

by

Bjørn Staghøj Knudsen
Martin Underlin Østergaard
Lars Bo Ibsen
Johan Clausen

June 2013

Scientific Publications at the Department of Civil Engineering

Technical Reports are published for timely dissemination of research results and scientific work carried out at the Department of Civil Engineering (DCE) at Aalborg University. This medium allows publication of more detailed explanations and results than typically allowed in scientific journals.

Technical Memoranda are produced to enable the preliminary dissemination of scientific work by the personnel of the DCE where such release is deemed to be appropriate. Documents of this kind may be incomplete or temporary versions of papers—or part of continuing work. This should be kept in mind when references are given to publications of this kind.

Contract Reports are produced to report scientific work carried out under contract. Publications of this kind contain confidential matter and are reserved for the sponsors and the DCE. Therefore, Contract Reports are generally not available for public circulation.

Lecture Notes contain material produced by the lecturers at the DCE for educational purposes. This may be scientific notes, lecture books, example problems or manuals for laboratory work, or computer programs developed at the DCE.

Theses are monograms or collections of papers published to report the scientific work carried out at the DCE to obtain a degree as either PhD or Doctor of Technology. The thesis is publicly available after the defence of the degree.

Latest News is published to enable rapid communication of information about scientific work carried out at the DCE. This includes the status of research projects, developments in the laboratories, information about collaborative work and recent research results.

Published 2013 by
Aalborg University
Department of Civil Engineering
Sohngaardsholmsvej 57,
DK-9000 Aalborg, Denmark

Printed in Aalborg at Aalborg University

ISSN 1901-7278
DCE Technical Memorandum No. 31

Determination of p-y Curves for Bucket Foundations in Sand Using Finite Element Modeling

Bjørn S. Knudsen[1] Martin U. Østergaard[1] Lars Bo Ibsen[2] Johan Clausen[3]

Department of Civil Engineering, Aalborg University

Abstract

Cylindrical offshore wind turbine foundations, such as bucket foundations and monopiles, have up till now been designed using analytical methods based on experiments done with piles much more slender than the ones used in today's industry. Compared to the widely used monopile foundation, the suction bucket has a much smaller ratio between length and diameter, and the suction buckets will thus act more as a rigid object during rotation in the soil. To improve the design of suction buckets through analytical methods, the soil pressure needs to be calculated more precisely since currently available $p-y$ curves, linking displacement and soil pressure, are based on more slender cylindrical structures. Using finite element methods, the $p-y$ curves for suction buckets will be determined as a function of the internal angle of friction of the soil, the diameter and the skirt length of the suction buckets, which can in turn be applied in determination of soil pressures for analytical design methods of suction bucket foundations.

1 Introduction

The aim of this study is to determine the soil pressure response p in drained sand as a function of a displacement y for a set of bucket foundations with different diameter D and skirt length L embedded in soils of varying strength determined by the internal angle of friction φ. The $p-y$ curves are found by using finite element modeling in PLAXIS 3D. PLAXIS 3D is used mainly within the fields of geotechnics since it has several advanced soil material models incorporated, e.g. the Hardening Soil Small Strain model that will be used in this investigation. The method used to obtain the soil response p and the displacement y is explained in the following.

1. A prescribed uniform horizontal displacement is applied to all parts of the bucket foundation. The soil reaction pressure p builds during this step, and p is extracted from PLAXIS 3D.

2. The horizontal displacement is removed from the bucket foundation so that only irreversible (i.e. plastic) deformations remain. This plastic deformation y is extracted from PLAXIS 3D.

3. This procedure is repeated for an increasing lateral displacement.

4. To increase usability of the results outside the finite element method, p and y are normalized to eliminate variation in depth and a function is fitted to allow for a fast computation of the soil reaction pressure p for varying bucket diameter, skirt length and soil strength (through the internal angle of friction φ).

2 Theory

Traditionally, soil response has been treated as a 2D-problem, described thoroughly for plane strain problems, e.g. sheet pile walls. With the introduction of monopiles as a solution to offshore foundation of e.g. wind turbines, the soil response of such cylindrical structures has increased the demands for knowledge within the field of 3D soil interaction. For a bucket foundation however, the existing knowledge regarding $p-y$ response curves for slender structures in 3D cannot be employed since buckets behave nearly rigid, cf. figure 1. Thus, the geometry has to be taken into account. The traditional 2D-theory provides a good offset for the understanding of displacement and soil response. Figure 2 shows how the active and passive earth pressure develop.

It can be seen that to mobilise the full passive soil pressure requires a larger displacement than to mobilise the full active pressure. The illustrated principle is valid for 2D but the same principle applies for 3D. To examine the 3D-effect, the soil pressure found in the numerical calculation will be compared to the 2D-soil pressure found by Rankine's soil pressure theory. By doing so, any added soil pressure obtained for a given displacement in a given soil compared to the 2D-case will be caused by this 3D-effect. Since the Rankine pressure is easily calculated, the results in the following

[1] *M.Sc. Student, Department of Civil Engineering, Aalborg University, Denmark*

[2] *Professor, Department of Civil Engineering, Aalborg University, Denmark*

[3] *Associate Professor, Department of Civil Engineering, Aalborg University, Denmark*

will mainly focus on determining the factor that the 3D-soil pressure is larger than the corresponding 2D-soil pressure.

3 Material Model

The applied material model in the finite element code is the Hardening Soil Small Strain material model (HSsmall). HSsmall includes the stress-dependent behaviour of the Hardening Soil Material Model (HS) where the current stress state is taken into account when calculating the stiffness, but HSsmall has a more realistic behaviour towards small strains. The HSsmall model is more demanding calculationwise, however the extra calculation time is well spend, as the results are closer to real-life behaviour. Additional stiffness at very small strains has long been known to occur in the field of soil dynamics, but has only recently been implemented in static calculations (Ovesen et al., 2009). By not using the HSsmall model there is a significant risk of overestimating the deformations in the soil and thus underestimating the stresses. Since the objective of this article is to find a link between the displacement y and the resultant soil pressure p, the HSsmall model is highly relevant. As the name implies the HSsmall model incorporates hardening in the soil, causing the stiffness parameters to change as a function of the current stress state. This is done by using a power law to describe the development of the moduli of elasticities and the shear moduli. The power laws for the different stiffness moduli follow the same form, e.g. the development of E_{50} is given by,

$$E_{50} = E_{50}^{ref} \left(\frac{\sigma_3 + c \cot(\varphi)}{\sigma_{\text{ref}} + c \cot(\varphi)} \right)^m . \quad (1)$$

The model incorporates a multi-surface yield criterion with isotropic hardening. The shape of the yield criterion is similar to that of the Mohr-Coulomb hexagonal cone, however the surface is bound by a cap in the direction of the hydrostatic stress axis. A sketch of the yield surface in the principal stress space is shown in figure 3. Compression is positive, tension is negative.

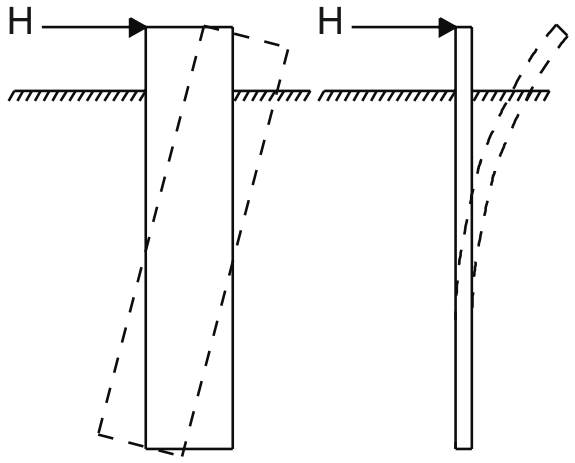

Figure 1: The difference between the behaviour of slender and non-slender piles when subjected to horisontal load. The non-slender pile rotates as a rigid body. (Brødbæk et al., 2009)

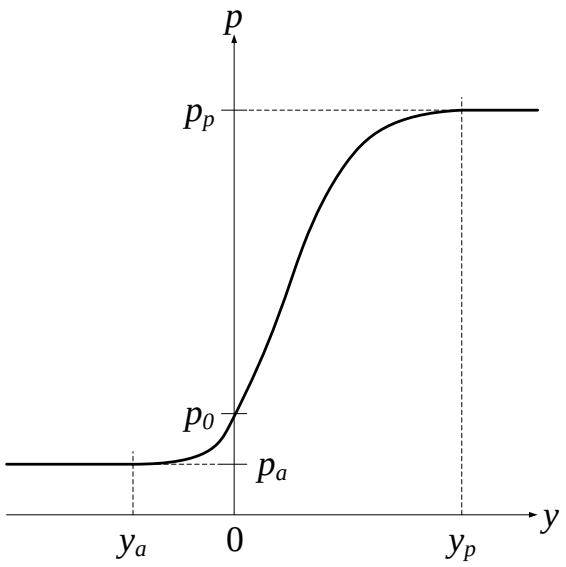

Figure 2: The relation between the displacement away from the soil δ_a and the active pressure p_a and the displacement towards the soil δ_p and the passive soil pressure p_p. The soil pressure at rest is p_0. (Ovesen et al., 2009)

4 Determination of Soil Strength and Stiffness Parameters

The internal angle of friction φ is commonly used as a design parameter for sands since it is used in Mohr-Coulomb yield criterion and also resembles a physical property of the material. Therefore, φ is also the main parameter in this study, and all other strength and stiffness parameters of the sand are linked to φ. The used relations in the following are taken from Det Norske Veritas (1992), Jensen et al. (2009) and Brinkgreve et al.

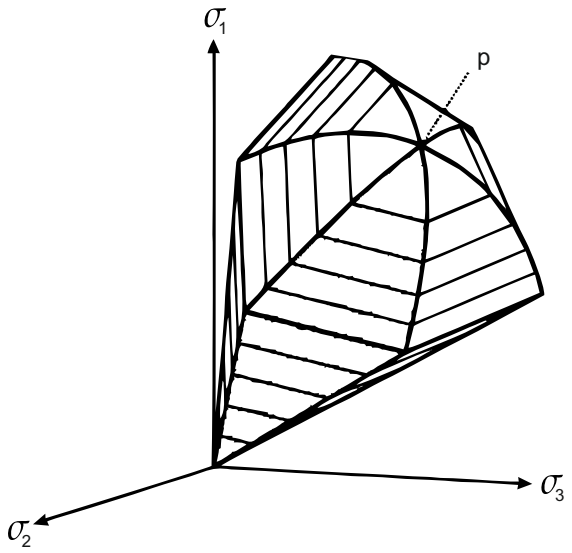

Figure 3: The yield surface of the HSsmall model. (Brinkgreve et al., 2012)

(2012) and the sand is assumed to be of the type *Frederikshavn Sand* which characteristics are typical for an offshore sand. The relative density I_D is an important parameter since it indicates how much the soil is compacted. The terms 'loose', 'medium' or 'dense' referring to the degree of compaction, is often used in empirical formulas in geotechnical engineering. I_D is linked to φ through,

$$\varphi = \varphi'_{crit} + 3^\circ I_R - 3^\circ I_D - \Delta\varphi_1, \tag{2}$$

where the critical internal of friction $\varphi'_{crit} = 33^\circ$, $\Delta\varphi_1 = 2^\circ$ for 5-10 % content of silt and I_R is calculated from,

$$I_R = I_D \left(Q_{min} - \ln \frac{p'}{1\ \text{kPa}} \right), \tag{3}$$

where the representative mean normal stress is $p' = 100$ kPa and $Q_{min} = 10$ for quartz sand. I_R and Q_{min} are both dependent on mineralogy of the grain material. Poissons ratio ν is linked to φ through,

$$\nu = \frac{1 - \sin\varphi}{2 - \sin\varphi}. \tag{4}$$

The elastic modulus E_{50} is determined from,

$$E_{50} = \frac{1 - \nu - 2\nu^2}{1 - \nu} E_{oed}, \tag{5}$$

with E_{oed} found by,

$$E_{oed} = m\sqrt{\sigma'\sigma_a}, \tag{6}$$

where m as a function of I_D is shown in figure 4. The values here are used commonly for Norwegian inorganic sands, which are assumed similar to Frederikshavn Sand. In equation (6), the atmospheric pressure is $\sigma_a = 100$ kPa and the reference pressure $\sigma' = 100$ kPa. This is used along with figure 4 to compute E_{oed}. For computing the unloading and reloading response, the unloading/reloading elastic modulus E_{ur} is calculated from,

$$E_{ur} = 3E_{50}. \tag{7}$$

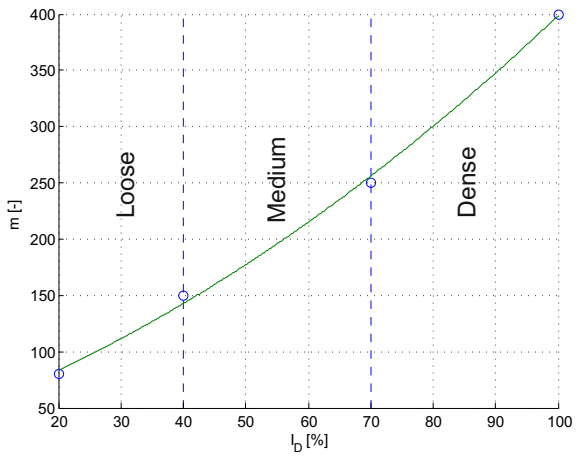

Figure 4: Approximation of m as a function of I_D. (Det Norske Veritas, 1992)

Table 1: Strength and stiffness parameters for sand used in the numerical model.

φ	[°]	30	35	40
ψ	[°]	0	5	10
Q_{min}	[-]	10.00	10.00	10.00
$\Delta\varphi_1$	[°]	2.00	2.00	2.00
I_D	[%]	15.17	53.09	91.02
ν	[-]	0.33	0.30	0.26
E_{50}	[MPa]	4.92	14.06	28.54
E_{oed}	[MPa]	7.39	18.87	35.15
E_{ur}	[MPa]	14.77	42.17	85.62
e	[-]	0.99	0.83	0.68
G_0	[MPa]	65.23	82.30	103.49
$\gamma_{0.7}$	[mm/m]	0.22	0.18	0.14
K_0	[-]	0.50	0.43	0.36
c'	[kPa]	0.10	0.10	0.10

In HSsmall extra parameters compared to HS need to be determined to model the stress dependency of the shear stiffness and the shear modulus dependency of the strain. The initial shear modulus G_0 is determined from equation (8) and the reference shear strain from equation (9).

$$G_0 = \frac{33\,(2.97 - e)^2}{1 + e}, \tag{8}$$

$$\gamma_{0.7} = \frac{2c'\,(1 + \cos(2\varphi')) - \sigma'_1\,(1 + K_0)\sin(2\varphi')}{9G_0}, \tag{9}$$

where the effective cohesion $c' = 0.1$ kPa and the coefficient for soil pressure at rest $K_0 = 1 - \sin(\varphi)$. The effective cohesion in the soil is set to 0.1 kPa to ensure numerical stability as recommended in Brinkgreve et al. (2012). $e_{min} = 0.64$ and $e_{max} = 1.05$ are used for the Frederikshavn Sand to determine e through,

$$I_D = \frac{e_{max} - e}{e_{max} - e_{min}}. \tag{10}$$

Table 1 contains the material parameters used in the numerical modeling in PLAXIS 3D.

5 Modeling in PLAXIS 3D

The finite element tool used to compute $p - y$ curves for the bucket foundation is PLAXIS 3D. The bucket is built using different geometries to determine the influence of the diameter D and the skirt length L on the $p - y$ response. The third changeable parameter is the internal angle of friction φ. Table 2 shows the models that are tested in PLAXIS 3D. The bucket itself is constructed of steel plate elements. The steel material is chosen thicker than steel ordinarily used for bucket foundations to increase the bending stiffness and to avoid any deformation in the steel structure itself. This is done since the main interest of this investigation is the soil response. To further avoid any bending in the bucket steel structure,

the displacement is applied to all parts of the bucket producing a lateral displacement of the entire bucket instead of the more realistic rotational behaviour. This does not influence the results, since only the lateral soil response is of interest.

5.1 Boundaries, Convergence and Meshing

The boundaries of the model domain are chosen so that the failure mechanism has enough room to develop fully without being influenced by the edges of the model. The size of the model domain is seen in figure 6. Along the bottom of the skirt, stress concentrations will arise due to the abrupt change in geometry. To even this concentration out and reduce the effect of it, an extended interface is introduced as recommended in Brinkgreve et al. (2012). The interface is extended both vertically and horizontally. The length of the extension is $L_{ext} = 0.2D$ based on Vaitkunaite (2012). To ensure the results close to the bucket, where the strain and stress gradients are large, are modeled with a sufficient accuracy, the mesh is refined in a volume close to the bucket itself. The size of this refined volume is shown in figure 6. The meshing facility in PLAXIS 3D allows for a relative meshing size to be chosen. Firstly the overall mesh density is selected, after which a linear mesh refinement factor is applied to the volume containing the bucket. A convergence analysis has been carried out, to ensure a sufficient mesh quality. An example of the mesh can be seen in figure 5.

Table 2: Overview of the tested models.

Model no.	D [m]	L [m]	φ [°]
1	10	5	30
2	10	5	35
3	10	5	40
4	10	10	30
5	10	10	35
6	10	10	40
7	15	7.5	30
8	15	7.5	35
9	15	7.5	40
10	15	15	30
11	15	15	35
12	15	15	40
13	20	10	30
14	20	10	35
15	20	10	40
16	20	20	30
17	20	20	35
18	20	20	40

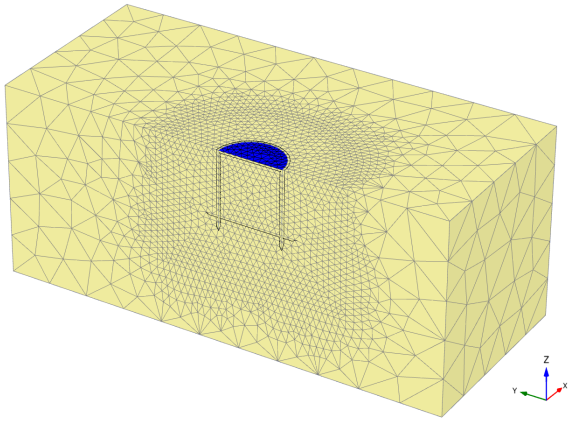

Figure 5: An example of the mesh of the FE model.

Table 3: Phases in the models.

Phase	Name	Action(s)
0	Initial	K_0-procedure, soil activated
1	Installation	Plates, interfaces activated
2	Nil-step	Equilibrium reestablished
3,5,7...	Load	Displacement activated
4,6,8...	Unload	Displacement deactivated

5.2 Phases in the Calculation

The model has five basic phases. The first two being the initial phase (phase 0) and installation phase (phase 1). In the nil-step phase, equilibrium is reestablished after the installation of the bucket and all deformations are reset because only the displacement from phase 3 and onwards is of interest. Phase 3 is a loading phase where the prescribed displacement is applied to all parts of the structure. Phase 4 is an unloading phase where the prescribed displacement is removed. Because of the elasto-plastic behaviour of the soil, the elastic deformations from phase 3 will be rolled back and only the plastic part of the deformation will remain. This pattern, plastic loading followed by elastic unloading, is continued for an increasingly large deformation until the soil body collapses or the maximum applied displacement has been reached.

5.3 Integration of Stresses

In order to determine the soil reaction pressure, the stresses on the bucket skirt are examined. From PLAXIS 3D it is possible to extract stresses in the soil, the plate elements of the bucket and the interface between soil and bucket. From Hansen et al. (2012) the method with extraction of stresses from the interface provided more reliable results and this method will be used in the following. In short, the method uses the normal σ'_N stress and the shear stresses τ_1 and τ_2 from the interfaces to compute a total soil pressure on the surface of the structure bucket foundation skirt as,

$$F_y = \int_A (\sigma_N \sin\theta + \tau_1 \cos\theta)\, dA. \tag{11}$$

The shear stress τ_1 acts along the circumference and τ_2 acts vertically along the skirt of the bucket. For determining the soil reaction pressure p, τ_2 is disregarded. The pressures acting on the bucket skirt during the horizontal displacement are shown in figure 7.

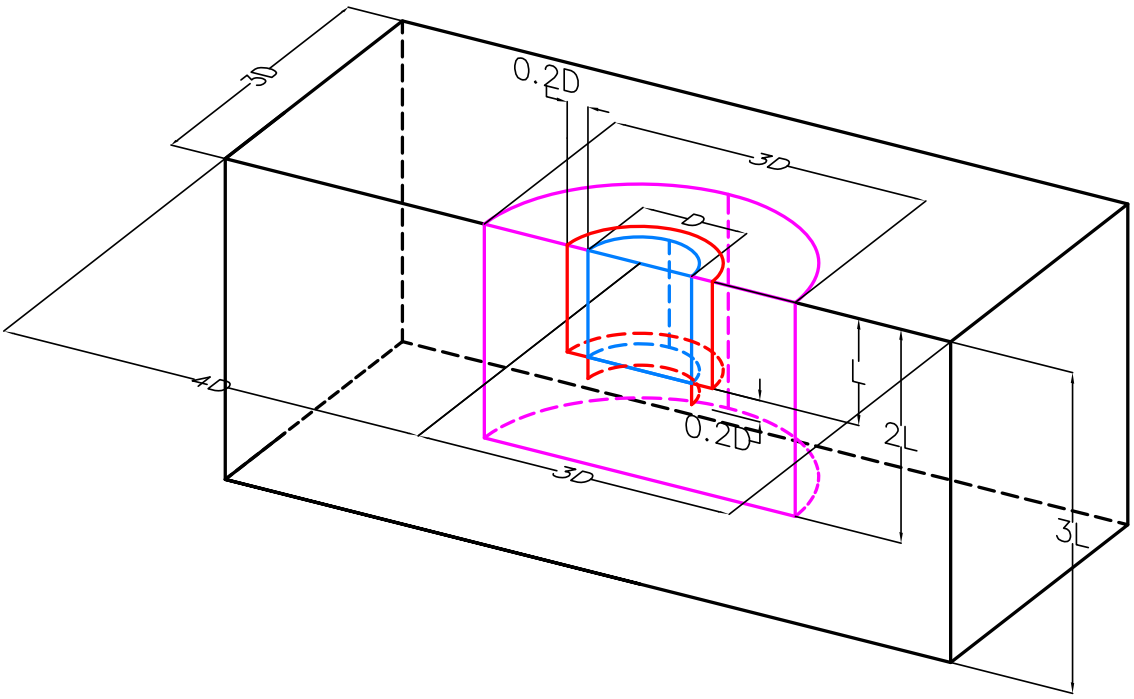

Figure 6: Size of model domain shown with black lines. The bucket itself is shown with blue lines, the volume with refined mesh is shown with pink lines and the extended interfaces are shown with red lines.

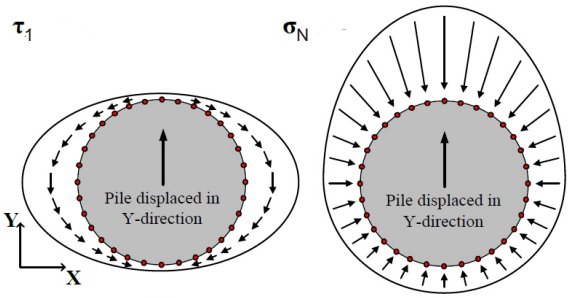

Figure 7: Principal sketch of the normal stress σ_N and the shear stress τ_1 when the bucket foundation is displaced horizontally (de Place, 2012).

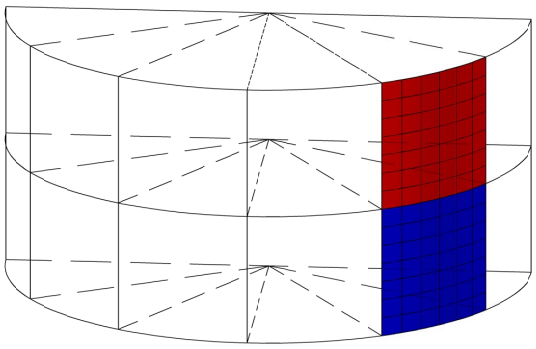

Figure 8: Areas for integration of surface stresses.

The bucket is divided into layers with the depth and each layer is divided into slices as seen in figure 8 where two areas, the blue and the red, have been highlighted as an example. In each of these areas, the average stress is found which is multiplied by the specific area to get the force acting on the specific area. The resulting soil reaction p for a given layer is then found as the sum of the average forces of all areas in this layer divided by the height of the layer.

6 Results

The results from the models shown in table 2 will be visualized through the following procedure.

1. Raw results from the model are plotted in a $p-y$ diagram.
2. The soil pressure p is normalized by the Rankine pressure p_R. The displacement y is normalized by the bucket diameter D.
3. The results are trimmed so edge effects in the skirt top and bottom are removed.
4. A tanh-function is fitted to the data.

6.1 Plotting of p-y Curves

The $p-y$ data extracted from model 9 is plotted in figure 9. There is a $p-y$ curve for each of the depth layers. The z-value in the legend is taken as the depth of the middle of each layer. The pressure increases with depth as expected. To better visualize the results, the depth parameter z is sought to be eliminated through normalization.

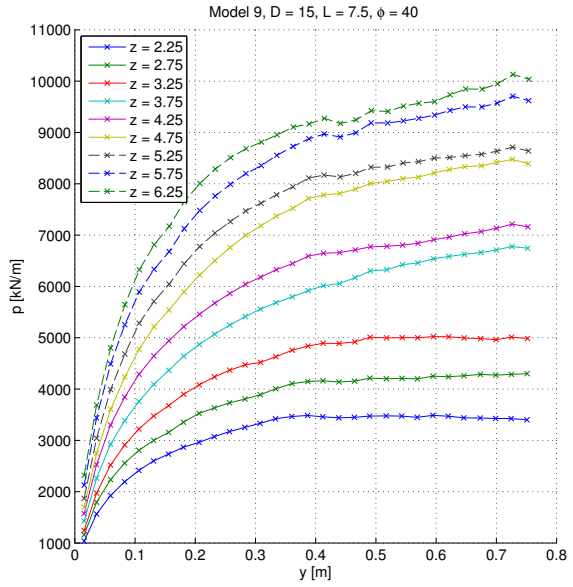

Figure 9: Step 1 - Raw results from the model are plotted in a $p-y$ diagram. This data have already been trimmed, cf. section 6.3.

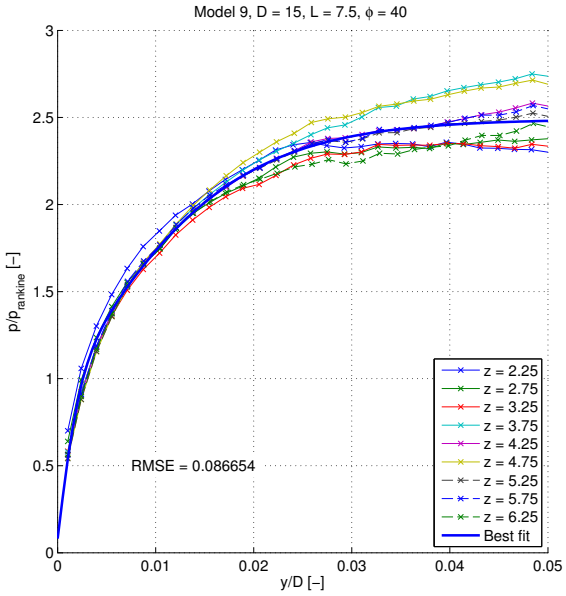

Figure 10: Step 3 and 4 - The results are trimmed so edge effects in the skirt top and bottom are removed. The best fit is shown.

6.2 Normalization of Soil Pressure

To eliminate the depth dependency of the $p-y$ curves, the soil pressure p is normalized by the Rankine pressure p_R which is a linear function of the depth z. The displacement y is normalized by the bucket diameter D. The Rankine pressure is calculated as,

$$\begin{aligned} p_R &= \gamma' z D (K_\gamma^p - K_\gamma^a) \\ &= \gamma' z D \left(\frac{1+\sin(\varphi)}{1-\sin(\varphi)} - \frac{1-\sin(\varphi)}{1+\sin(\varphi)} \right), \end{aligned} \tag{12}$$

where γ' is the specific soil weight, z is the depth and φ is the internal angle of friction of the soil. By normalizing the pressure p by the Rankine pressure that is a linear function of the depth z, the $p-y$ curves for each depth layer will turn into one curve, if the pressure p is also a linear function of z.

6.3 Trimming and Fitting of Data

It is evident from investigating the data, that the normalization by the Rankine pressure is not suitable in the top and the bottom of the bucket. These variations are considered to be edge effects and are disregarded. After the data has been trimmed, the results are fitted with a function of the type,

$$\begin{aligned} \frac{p}{p_R} &= \beta_1 \tanh\left(\beta_2 \frac{y}{D}\right) \\ &\quad + \beta_3 \tanh\left(\beta_4 \frac{y}{D}\right) + \frac{K_0}{K_\gamma^p - K_\gamma^a}, \end{aligned} \tag{13}$$

where β_2 and β_4 are shape coefficients of the fitting function that controls the climb rate of the function in the initial part and towards the ultimate soil pressure. From

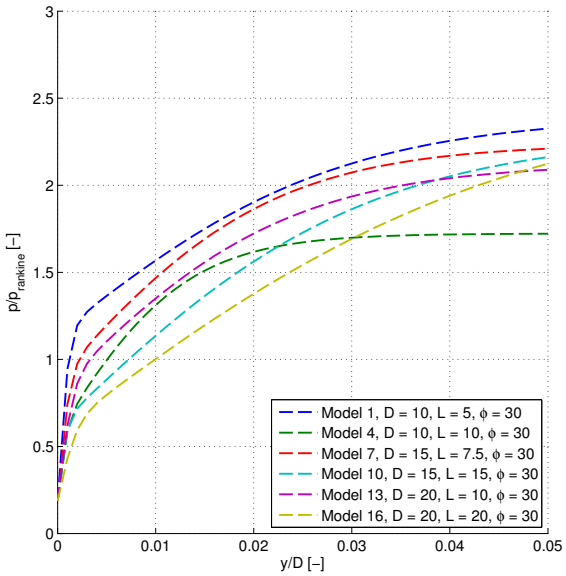

Figure 11: Best fit for models with $\varphi = 30°$.

equation (13) it is evident that,

$$\frac{p}{p_R} \to \beta_1 + \beta_3 + \frac{K_0}{K_\gamma^p - K_\gamma^a} \quad \text{for} \quad \frac{y}{D} \to \infty, \tag{14}$$

meaning that β_1 and β_3 control the maximum relative soil pressure. The fitting function consists of three terms, the first two enabling the fitting function to fit both the initial and end slope, while the third term involving K_0 takes into account the soil pressure at rest at $y = 0$. The trimmed data with the fitted function is shown in figure 10. This procedure is done for all 18 models, and the fitted functions are gathered - one diagram for $\varphi = 30°$, $\varphi = 35°$ and $\varphi = 40°$. These results are shown in figures 11, 12 and 13. From this initial study of the $p-y$ curves and the best fit, it seems like models with $L/D = 0.5$ have

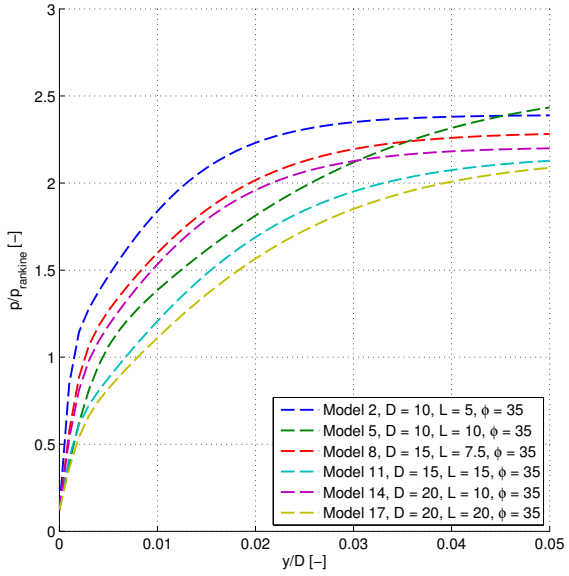

Figure 12: Best fit for models with $\varphi = 35°$.

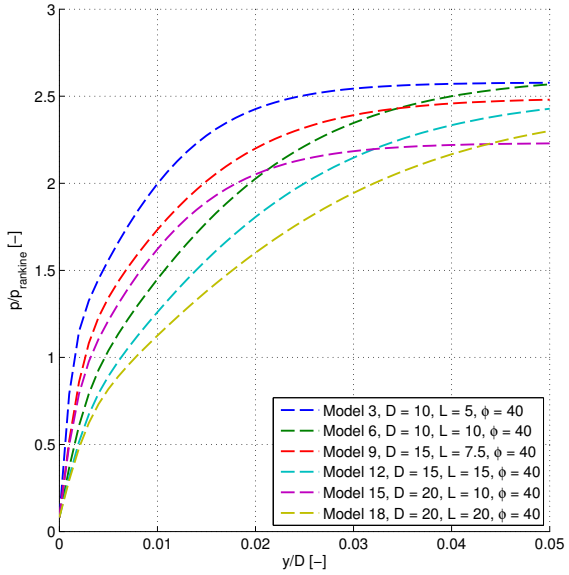

Figure 13: Best fit for models with $\varphi = 40°$.

a bigger initial stiffness than models with $L/D = 1$. This is evident for all values of φ. Figures 11, 12 and 13 show the best fit, meaning that the parameters β_1, β_2, β_3 and β_4 are free to attain an arbitrary value. In the following, these parameters are sought to be described as a function of the three basic parameters, D, L and φ.

7 Mathematical Model

In order to put the results from the numerical examination into real-life application, a mathematical model, that can be used to evaluate the soil response of an arbitrary bucket geometry and soil strength, is sought. The method for obtaining this mathematical expression is to examine the dependency of the parameters β_1 to β_4 of the geometrical parameters D and L and the soil strength

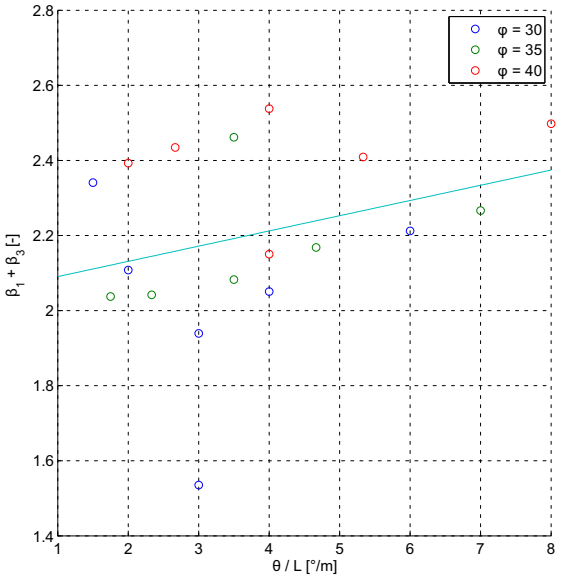

Figure 14: Examination of $\beta_1 + \beta_3$ as a function of $\frac{\varphi}{L}$.

Table 4: Coefficients in the fit of β_1 and β_3.

a_1 $\left[\frac{m}{°}\right]$	a_2 $[-]$	b_1 $\left[\frac{m}{°}\right]$	b_2 $[-]$
0.041	2.050	0.107	0.560

parameter φ. Ultimately, the goal is to express the earth pressure through D, L and φ.

7.1 Investigation of β_1 and β_3

The parameters β_1 are β_3 are investigated as a pair, since they both contribute to the limit value for y/D going towards infinity as described in section 6.3. The investigation of β_1 and β_3 is done by plotting the sum $\beta_1 + \beta_3$ and the product $\beta_1\beta_3$ against the basic parameters D, L and φ to discover any trend in the data. To get the actual values for β_1 and β_3, two equations with two unknowns have to be solved. In this particular case, it is seen that the sum and product could be described as linear functions of the types,

$$\beta_1 + \beta_3 = a_1 \frac{\varphi}{L} + a_2, \tag{15}$$

$$\beta_1\ \beta_3 = b_1 \frac{\varphi}{L} + b_2. \tag{16}$$

Figures 14 and 15 show the data and the best linear fit. The coefficient for the two linear functions are seen in table 4.

7.2 Investigation of β_2 and β_4

Subsequently to examining the linear fit of β_1 and β_3, these two parameters are locked in the non-linear fitting. This means that the non-linear fit is done again, this time only for β_2 and β_4. The slope parameters β_2 and β_4 are

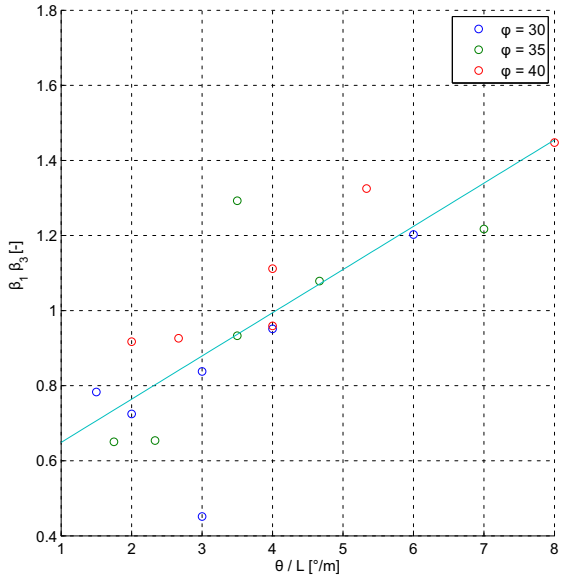

Figure 15: Examination of β_1 β_3 as a function of $\frac{\varphi}{L}$.

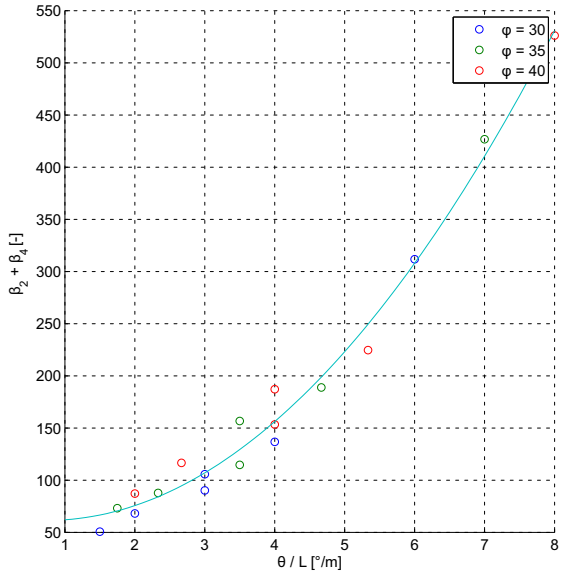

Figure 16: Examination of $\beta_2 + \beta_4$ as a function of $\frac{\varphi}{L}$.

examined using the same procedure as for β_1 and β_3, using the sum and the product. From the examination, it is found that the best fit for β_2 and β_4 are found to be a polynomial fit in the form,

$$\beta_2 + \beta_4 = c_1 \left(\frac{\varphi}{L}\right)^2 + c_2 \left(\frac{\varphi}{L}\right) + c_3, \qquad (17)$$

$$\beta_2 \, \beta_4 = d_1 \left(\frac{\varphi}{L}\right)^2 + d_2 \left(\frac{\varphi}{L}\right) + d_3, \qquad (18)$$

Again, the coefficients of the fit are found. They can be seen in table 5. The actual plot of the data and the best quadratic fit can be seen in figures 16 and 17.

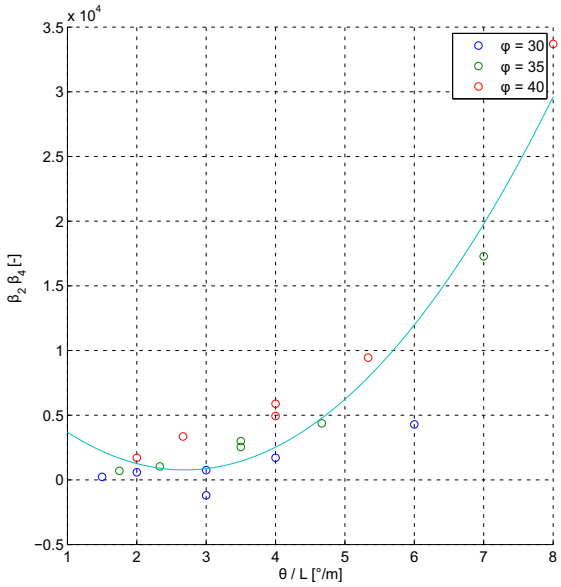

Figure 17: Examination of β_2 β_4 as a function of $\frac{\varphi}{L}$.

Table 5: Coefficients in the fit of β_2 and β_4.

c_1 $\left[\left(\frac{m}{°}\right)^2\right]$	c_2 $\left[\frac{m}{°}\right]$	c_3 $[-]$	d_1 $\left[\left(\frac{m}{°}\right)^2\right]$	d_2 $\left[\frac{m}{°}\right]$	d_3 $[-]$
8.900	-13.12	66.24	936.5	-4579	5989

7.3 Assessment of Mathematical Model

After developing the mathematical model it is compared to the best fit done by non-linear curve fitting. Figure 18 shows the two functions and the original data. It shows relatively good coherence between the best fit and the mathematical model. The quality of the fit based on the mathematical model of course varies, but in general the quality is good. The worst results are gained from the models with $\varphi = 30°$. Obviously, greater effort could be put into the development of this mathematical model - especially regarding the connection between the basic parameters, D, L and φ, and the fitting parameters, β_1, β_2, β_3 and β_4. In this case, the fitting parameters were examined as a function of D, L, φ, φ/D and φ/L, and as shown, the coherence was best in the case of φ/L. No significant trend based on the bucket diameter D was found. This matter should be examined further. Ultimately, the mathematical model is rather simple even though it uses ten fitted parameters as input. A more precise model could possible be developed, but it would without any doubt involve substantially more complex expressions. The user should assess whether this formulation is adequate for use in the specific case.

8 Conclusion

From the numerical analysis of the lateral displacement of the bucket foundation and the corresponding soil response in the drained condition, a general expression

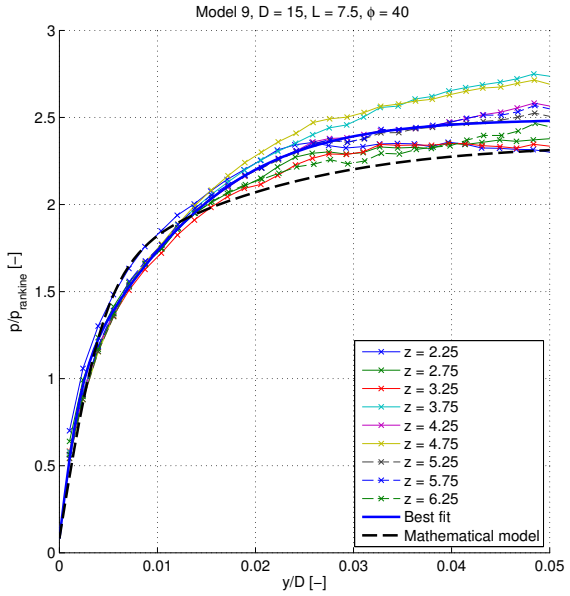

Figure 18: Comparison between best fit with free parameters and the mathematical model.

for obtaining the soil pressure is given for an arbitrary bucket diameter, bucket skirt length and internal angle of friction of the surrounding soil. This enables fast computation of the soil pressure to be used in analytical design models. When designing numerous bucket foundations for e.g. an offshore wind turbine park, it is important that the stabilising pressures on the skirt sides can be calculated readily but still accurately enough to provide a safe but still efficient design.

9 Further Work

In the formulation of the mathematical model, ten empirical parameters were necessary. Further calibration of these parameters by doing more models with varying geometry and strength parameters is a straight-forward expansion of the investigations and could help increase the validity of the formulation. The numerical tests done in this project have all been drained tests for a typical offshore sand. A natural way to expand the work and obtain further results, would be to perform the same tests in the undrained condition. In nature, the behaviour of the bucket foundation will be much influenced by the build up and dissipation of pore pressure in and around the bucket skirts. However, in nature neither completely drained or undrained conditions can be assumed - this depends solely on the nature of the loading. A more probable scenario is that the actual behaviour is somewhere in between completely drained and undrained - namely partially drained. The partially drained state will be examined in a scaled experiment in the pressure tank at Aalborg University in the Spring 2013. This project will try to clarify the behaviour of the bucket foundation when subjected to loading with varying velocity.

References

Brinkgreve, Engin, and Swolfs, **2012**. R.B.J. Brinkgreve, E. Engin, and W.M. Swolfs. *Manual for PLAXIS 3D 2012*, 2012.

Brødbæk, Møller, Sørensen, and Augustesen, **2009**. K.T. Brødbæk, M. Møller, S.P.H. Sørensen, and A.H. Augustesen. *Review of p-y relationships in cohesionless soil.* 2009.

Place, **2012**. Jesper Brade de Place. *Assessment of p-y curves for monopile foundations*, 2012.

Det Norske Veritas, **1992**. Det Norske Veritas. *Foundations: Classification Notes no. 30.4*, 1992.

Hansen, Rasmussen, and Wolf, **2012**. Mette Hansen, Kristian Lange Rasmussen, and Torben Kirk Wolf. *Assessment of p-y Curves from Numerical Methods for a Non-Slender Monopile in Cohesionless Soil*. 2012.

Jensen, Mohr, Mortensen, Hansen, Hansen, Sørensen, Bager, Laustsen, Plum, Svensson, Søndergaard, Adelhøj, Munch-Andersen, Cornelius, Hansen, Goltermann, Steenfelt, Sørensen, and Borchersen, **2009**. Bjarne Chr. Jensen, Gunnar Mohr, Bo Mortensen, Lars Pilegaard Hansen, Svend Ole Hansen, Finn Olaf Precht Sørensen, Dirch H. Bager, Henning Laustsen, Carsten Munk Plum, Eilif Svensson, Ejnar Søndergaard, Johan Adelhøj, Jørgen Munch-Andersen, Thomas Cornelius, Lars Zenke Hansen, Per Goltermann, Jørgen S. Steenfelt, Carsten S. Sørensen, and Egil Borchersen. *Teknisk Staabi*. Nyt Teknisk Forlag, 20. edition, 2009.

Ovesen, Fuglsang, and Bagge, **2009**. Niels Krebs Ovesen, Leif Fuglsang, and Gunnar Bagge. *Lærebog i Geoteknik*. 978-87-502-0961-4. Polyteknisk Forlag, 2009.

Vaitkunaite, **2012**. Evelina Vaitkunaite. *Guidelines for length of extended interfaces for bucket foundations*. 2012.

Recent publications in the DCE Technical Memorandum Series

DCE Technical Memorandum no. 31, Determination of p-y Curves for Bucket Foundations in Sand Using Finite Element Modeling, Bjørn Staghøj Knudsen, Martin Underlin Østergaard, Lars Bo Ibsen and Johan Clausen, June 2013.

DCE Technical Memorandum no. 32, Implementation of a Stress-dependent Strength Material Model in PLAXIS 3D, Bjørn Staghøj Knudsen, Martin Underlin Østergaard and Johan Clausen, June 2013.

DCE Technical Memorandum no. 33, Small-scale Testing of Bucket Foundations in Sand, Bjørn Staghøj Knudsen, Martin Underlin Østergaard and Lars Bo Ibsen, June 2013.

ISSN 1901-7278
DCE Technical Memorandum No. 31